A novel transferrin/TfR2-mediated mitochondrial iron transport system is disrupted in Parkinson's disease

Pier Giorgio Mastroberardino[a,b,*], **Eric K. Hoffman**[a,b], **Maxx P. Horowitz**[c], **Ranjita Betarbet**[e], **Georgia Taylor**[e], **Dongmei Cheng**[f], **Hye Mee Na**[a,b], **Claire-Anne Gutekunst**[e], **Marla Gearing**[g], **John Q. Trojanowski**[h], **Marjorie Anderson**[i], **Charleen T. Chu**[b,d], **Junmin Peng**[f], and **J. Timothy Greenamyre**[a,b]

[a]Department of Neurology, University of Pittsburgh, 3501 fifth avenue, Pittsburgh, PA 15260, USA

[b]Pittsburgh Institute for Neurodegenerative Diseases, USA

[c]Medical Scientist Training Program and Center for Neuroscience, University of Pittsburgh, USA

[d]Department of Pathology, University of Pittsburgh, Pittsburgh, PA 15213, USA

[e]Department of Neurology, Center for Neurodegenerative Disease, Emory University, Atlanta, GA 30322, USA

[f]Department of Human Genetics, Center for Neurodegenerative Disease, Emory University, Atlanta, GA 30322, USA

[g]Department of Pathology, Center for Neurodegenerative Disease, Emory University, Atlanta, GA 30322, USA

[h]Center for Neurodegenerative Disease Research, University of Pennsylvania, Philadelphia, PA 19104, USA

[i]University of Washington, Department of Rehabilitation Medicine, Seattle, WA 98195, USA

Abstract

More than 80 years after iron accumulation was initially described in the substantia nigra (SN) of Parkinson's disease (PD) patients, the mechanisms responsible for this phenomenon are still unknown. Similarly, how iron is delivered to its major recipients in the cell – mitochondria and the respiratory complexes – has yet to be elucidated. Here, we report a novel transferrin/transferrin receptor 2 (Tf/TfR2)-mediated iron transport pathway in mitochondria of SN dopamine neurons. We found that TfR2 has a previously uncharacterized mitochondrial targeting sequence that is sufficient to import the protein into these organelles. Importantly, the Tf/TfR2 pathway can deliver Tf bound iron to mitochondria and to the respiratory complex I as well. The pathway is redox-sensitive and oxidation of Tf thiols to disulfides induces release from Tf of highly reactive ferrous iron, which contributes to free radical production. In the rotenone model of PD, Tf accumulates in dopamine neurons, with much of it accumulating in the mitochondria. This is associated with iron deposition in SN, similar to what occurs in PD. In the human SN, TfR2 is also found in mitochondria of dopamine neurons, and in PD there is a dramatic increase of oxidized Tf in SN. Thus, we have discovered a novel mitochondrial iron transport system that goes awry in PD, and which may provide a new target for therapeutic intervention.

*Corresponding author. Department of Neurology, University of Pittsburgh, 3501 fifth avenue, Pittsburgh, PA 15260, USA. Fax: +1 412 648 9766. *E-mail address:* mastroberardinopg@upmc.edu (P.G. Mastroberardino).

Keywords

Parkinson's disease; Rotenone; Oxidative stress; Mitochondria; Iron; Transferrin

Introduction

The redox properties and coordination chemistry of iron make it ideally suited for a variety of biological functions (Huang et al., 2006); these same properties make it potentially dangerous, by virtue of its ability to generate reactive oxygen species (Halliwell and Gutteridge, 1999). Therefore, iron transport, storage, and levels in cytoplasm and organelles must be tightly coordinated and controlled. The majority of cellular iron is directed to mitochondria, in part because of their high content of iron–sulfur clusters, which are essential for mitochondrial respiration (Huang et al., 2006). Complex I of the electron transfer chain alone contains 8 iron–sulfur complexes (Hatefi, 1985).

Several hereditary neurodegenerative disorders, including neuro-ferritinopathy(Curtis et al., 2001), neurodegeneration with brain iron accumulation (NBIA) (Zhou et al., 2001) and Friedreich's ataxia (Campuzano et al., 1996) are caused by abnormal iron homeostasis – and each is associated with a variable mitochondrial defect. In fact, the gene products responsible for NBIA and Friedreich's ataxia are nuclear-encoded mitochondrial proteins, underscoring the importance of mitochondria in iron homeostasis.

Parkinson's disease (PD) is a common neurodegenerative disorder that is associated with degeneration of dopaminergic neurons in the substantia nigra. Although the etiology of parkinsonian neurodegeneration is complex, there is strong evidence that mitochondrial impairment and oxidative stress play key roles in PD pathogenesis (Greenamyre and Hastings, 2004). Indeed, selective partial inhibition of mitochondrial electron transfer at the level of complex I accurately reproduces many features of the disease (Betarbet et al., 2000; Przedborski et al., 2001).

The normal substantia nigra has a higher concentration of iron than the liver, which is the body's main iron store (Gotz et al., 2004). Markedly increased levels of iron in the parkinsonian substantia nigra were described initially in 1924 – far before the discovery of dopamine deficiency in the early 1950s (Iversen and Iversen, 2007) – and confirmed by numerous other consequent studies (Berg and Hochstrasser, 2006). A potential role for iron accumulation in PD pathogenesis is supported by the fact that mutations in genes related to iron homeostasis are associated with a higher relative risk for developing PD (Borie et al., 2002; Guerreiro et al., 2006). In addition, iron chelation protects substantia nigra neurons in animal models of PD (Ben-Shachar et al., 1991; Kaur et al., 2003). A recent neuropathological study has demonstrated for the first time that iron is elevated within substantia nigra dopamine neurons, possibly secondary to mitochondrial impairment (Oakley et al., 2007). Despite the importance of iron in mitochondrial function and its potential role in PD pathogenesis, our understanding of how iron accumulates in neurons and how it is transported into mitochondria is rudimentary.

In the studies reported here, we have explored the mechanisms responsible for iron accumulation in substantia nigra dopamine neurons in the rotenone model of PD. In so doing, we have discovered a novel mitochondrial iron transport system involving transferrin (Tf) and transferrin receptor 2 (TfR2). Disruption of this system in the rotenone model leads to transferrin and iron accumulation in substantia nigra, and the same process appears to occur in the human brain in PD.

Methods

Materials

All reagents were from Sigma, unless otherwise specified. Paraffin embedded sections of human brain were obtained from the Emory University, the University of Pittsburgh brain banks and from the University of Pennsylvania Alzheimer's Disease Core Center and Neuropathology Core. A total of 12 sporadic PD cases and 6 controls were analyzed. The mean age was 78±7.9 years for the PD cases and 77± 4.3 years for the controls. The mean post-mortem time was 8±4.3 h for the PD cases and 12±7.2 h for the controls.

Antibodies

Antibodies were used at the following concentrations: Western blot: Trf (VAP-EN004, Stressgen, Victoria, BC, Canada) 1:5000, mitochondrial complex I 39 kDa subunit (Molecular Probes, Eugene, OR, USA) 1:5000, Transferrin receptor 2 (Tfr21-A Alpha Diagnostic San Antonio, TX, 1:500 or PAB-11168 and PAB 11169, Orbigen, San Diego, CA, 1:100 or 9F8-1C11, Abcam, Cambridge, MA 1:500), MnSOD (Calbiochem, San Diego, CA, USA) 1:1000, Tom20 (BD Biosciences, San Jose, CA, USA) 1:2500, cytochrome c (BD Biosciences, San Jose, CA, USA) 1:500. Immunohistochemistry: TH (MAB318, Chemicon Temecula, CA, 1:2000), OX42 (MCA 275G AbD Serotec, Oxford, UK, 1:150), IBA-1 (Wako, Richmond, VA), CD68 (EMB11, Dako, Ely, United Kingdom, 1:200), TfR1 (H68.4, Zymed laboratories, Invitrogen, Carlsbad, CA, 1:500), TfR2 (Tfr21-A, Alpha Diagnostic, San Antonio, TX, 1:500 or 9F8 1C11, Abcam, Cambridge, MA, 1:100), GFAP (MAB 3402 or AB5804, Chemicon, Temecula, CA 1:1000 and 1:2000 respectively), transferrin (VAP-EN004, Stressgen, Victoria, BC, Canada, 1:1000), human mitochondrial antigen (Biogenex, San Ramon, CA, 1:10), Hsp70 (SPA-812, Stressgen, Victoria, BC, Canada, 1:4000), Hsp60 (SPA-806, Stressgen, Victoria, BC, Canada, 1:1000).

Primary antibody labeling

In some experiments, it was necessary to directly label primary antibodies rather than using secondary antibodies. This was carried out using the DyLight 547 and 647 antibody labeling kit (Pierce, Rockford, IL), or Alexa488 labeling kit (Molecular Probes, Eugene, OR). Lyophilized primary antibody was resuspended in 0.05 M borate buffer, pH 8.5, to a final concentration of 1 mg/ml and 100 µg was used for labeling. The dyes were reconstituted in 20 µL of dimethylformamide; 8 µL of DyLight 547 or 5 µL and DyLight 647 were added to the antibody solution and the mixture was incubated for 45 min at room temperature. The antibody was purified and the excess dye was removed by processing the solution with a Micro Bio-Spin chromatography column 6 (Biorad, Hercules, CA); the antibody solution was applied to the center of the column and then centrifuged at room temperature for 4 min at 1000 ×g. After chromatography, the antibody was in 10 mM TrisHCl buffer, pH 7.4, ready for use.

Rotenone treatment and mitochondrial purification and analysis

All animal use followed the University of Pittsburgh Institutional Animal Care and Use Committee approved protocols. Lewis rats were treated with rotenone as previously described (Betarbet et al., 2006; Betarbet et al., 2000). Animals were deeply anesthetized and euthanized by decapitation. Brains were divided mid-sagittally and one-half was post-fixed for histological studies and the other half was used for biochemical and mitochondrial studies. Brain regions of interest were microdissected quickly and homogenized on ice in 0.32 M sucrose, 30 mM TrisHCl pH 7.4,1 mM EDTA, using a teflon-glass homogenizer. The sample was centrifuged (900 ×g, 10 min, 4 °C) to remove nuclei and debris and the supernatant was centrifuged again (10,000 ×g, 15 min, 4 °C). The pellet was resuspended in 3 mL of 0.32 M sucrose, 30 mM TrisHCl pH 7.4, 1 mM EDTA. The sample was then layered on top of a discontinuous gradient

(3 mL of 0.8 M sucrose, 30 mM TrisHCl, pH 7.4 and 3 mL of 1.2 M sucrose 30 mM TrisHCl pH 7.4). After centrifugation in a SW41Ti rotor (Beckman, 2 h, 53,000 g, 4 °C), the band containing mitochondria at the interface of the 0.8 M/1.2 M layers was collected and diluted with two volumes of TrisHCl pH 7.4. Alternatively, mitochondria were prepared using percoll gradients as previously reported (Panov et al., 2002). The two different mitochondrial preparation protocols gave identical results; purity of mitochondria was assessed by western blot (Supplemental Fig. 8). Mitochondria were centrifuged and used immediately. Mitochondrial subfractionation was carried out as described by others (Hovius et al., 1990). Trypsin digestion of intact mitochondria was carried out as previously described (Choo et al., 2004), using different amounts of enzyme (Sigma, St. Louis, Mo, about 10,000 BAEE units per milligram of protein) as indicated in Fig. 2e. The reaction was stopped by adding protease inhibitors. Western blot analysis was carried out according to standard procedures (Betarbet et al., 2006).

In addition to studies in rats, 3 monkeys (2 *Macaca fascicularis* and 1 *Macaca mulatta*) were treated chronically with rotenone. In brief, the monkeys were treated with rotenone for 18 or 19 months and their brains were processed for histology. Two of three monkeys exhibited selective loss of nigrostriatal dopaminergic nerve terminals and accumulation of α-synuclein in the substantia nigra. Although the third monkey did not show frank nigrostriatal degeneration, when examined blindly, it had extensive microglial activation and iron deposition in the substantia nigra compared to control monkeys.

Histology

Immunohistochemistry and immunofluorescence were performed on paraformaldehyde fixed section as previously described. To eliminate endogenous fluorescence, monkey and human tissues were pre-treated with an autofluorescence eliminating reagent according to the manufacturer's instructions (Chemicon, Temecula, CA, Supplemental Fig. 9). Images were acquired using a laser scanning confocal microscope (Fluoview FV1000, Olympus, Japan) or Leitz microscope (Leica, Wetzlar, Germany). Quantification of fluorescence intensity in human specimens (Fig. 7c) was performed with the Olympus Fluoview FV1000 software. For each specimen (*n*=4 controls, *n*=6 PD), three different fields were averaged. Histochemical detection of non-heme iron was performed as described (Smith et al.,1997); in brief, following standard immunocytochemistry procedures, the sections were washed in dH_2O and incubated in equal parts mixture of 20% HCl and 10% K_4Fe (CN)$6 \times 3H_2O$ for 20 min. Then the sections were washed in dH_2O and mounted from PBS. Immuno-electron microscopy was performed as previously described (Gutekunst et al., 1999). FRET between DyLight 547 and DyLight 647 to establish Tf-TfR2 proximity (Kenworthy, 2001) was measured detecting the emission of the acceptor (DyLight 647) upon excitation of the donor (DyLight 547) using a laser scanning confocal microscope (Fluoview 1000, Olympus, Japan).

Histological labeling of oxidized thiols

All steps were carried out at room temperature unless indicated otherwise, as previously described (Mastroberardino et al., 2008). Fixed cells or brain sections were washed 3 times for 10 min in phosphate buffered saline pH 7.2 (PBS) and then free thiols were blocked by incubating the samples for 60 min with PBS containing 100 mM iodoacetamide and 100 mM N-ethylmaleimide. Samples were then washed 3 times for 10 min in PBS. Thiols in the form of disulfides were reduced by incubating the samples for 30 min in PBS containing 4 mM tributylphosphine (TBP); TBP was omitted in the control reaction. Samples were rinsed in PBS to remove TBP.

The following steps were performed in the dark: Reduced thiols (from what were previously disulfides) were fluorescently labeled by incubating the samples for 2 h with freshly prepared

1 mM anilino-naphtalene sulfonate maleimide (Molecular Probes, Eugene, Oregon). Samples were washed 3 times for 10 min in PBS.

In most cases, sections were also double labeled using immuno-fluorescence. The following steps resemble a standard immunohisto-chemistry procedure: samples were blocked with 5% goat serum in PBS for 30 min at room temperature and then were incubated overnight at 4 °C with the primary antibody solution. It was necessary to use a primary antibody conjugated to a FITC derivative (i.e. Alexa488, Molecular Probes, Eugene, Oregon) in order to study the transfer of energy (FRET)between the thiol dye and the immuno-labeled protein of interest. After three washes in PBS, 10 min each, the samples were mounted on slides using an anti-fade medium (0.1 M propyl gallate in PBS–50% glycerol). Images were acquired using a laser scanning confocal microscope (Fluoview1000, Olympus). Parameters were set with the control reaction (reaction without TBP) and applied for all the analysis.

FRET was detected by reading the acceptor emission (FITC derivative-conjugated primary antibody) at 520 nm while exciting the donor (anilino-naphtalene sulfonate maleimide) with the 405 nm laser. The following control experiments were performed: in one set of cells the reducing step (TBP) was omitted; therefore, no free thiols were available for the labeling with the fluorescent maleimide. In a second experiment, samples were stained for β-synuclein, which does not contain a cysteine residue and can therefore be used as a negative control. In each case, there was no FRET signal.

Detection of Tf redox-sensitive thiols

Redox buffers were prepared in TrisHCl pH 7.4, 0.5 M, mixing oxidized and reduced glutathione as previously described (Watson et al., 2003). 50 µg of Tf was incubated in redox buffers for 1 h at room temperature. Free thiols were derivatized with 1 mM of N-ethylmaleimide-conjugated polyethyleneglycol (NEM-PEG, SunBio, Orinda, CA) added directly to the SDS loading buffer. The sample was resolved by SDS-electrophoresis according to standard procedures. The gel was stained with colloidal Coomassie, 0.2% G-250 Coomassie (SERVA, Heidelberg, Germany) dissolved in 35% methanol, 3.5% ortophosphoric acid, 1.3 M ammonium sulfate.

Identification and quantification of oxidized thiols by ICAT

Mitochondria (0.1mg) were resuspended and solubilized in 100 mM TrisHCl, pH 7.4, 1% SDS (Tris/SDS) at a final concentration of 1 mg/ml. Proteins were denatured by heating the solution at 70 °C for 5 min.

N-ethylmaleimide and iodoacetamide were added at a final concentration of 50 mM each. The mixture was incubated for 30 min at 37 °C and precipitated with 5 volumes of ice-cold precipitation solution (50% acetone, 25% methanol, 25% ethanol, for 1 h at – 80 °C). After spinning for 25 min (3200 ×g, 4 °C), the pellet was resuspended in 1 ml Tris/SDS; cysteines that were previously engaged in disulfide bonds were reduced with TBP in dimethylformamide (20 mM final concentration). The mixture was incubated for 15 min at RT. Proteins were precipitated again with ice-cold acetone and the newly revealed thiols were labeled with cleavable ICAT reagents according to the manufacturer's protocol (Applied Bio-systems, Framingham, MA). The reduced mitochondrial proteins from substantia nigra, with or without rotenone treatment, were labeled with ICAT heavy and light reagents, respectively. The labeled proteins were then combined and then digested with 2 µg of trypsin (Promega, Madison, WI) overnight. The resulting peptides were isolated with a strong-cation exchange cartridge and biotin-labeled peptides were affinity-purified with an avidin cartridge and dried in a SpeedVac. The biotin moiety of labeled peptides was then removed using Cleaving Reagent (Applied Biosystems). Finally, the samples were dried and used for mass spectrometry (Supplemental

Fig. 3). The cleaved ICAT-labeled peptides were dissolved and analyzed by capillary reverse-phase liquid chromatography-tandem mass spectrometry (LC-MS/MS), details of which were described previously (Gygi et al., 1999; Liao et al., 2004). A database search revealed the identity of ICAT-labeled Cyscontaining peptides; the results were further validated by manually examining their MS/MS spectra. Quantification of labeled peptides was carried out by comparing the peak areas of corresponding peptides (heavy vs. light) in the same MS survey scan.

Cloning the Tfr2 mitochondrial targeting sequence

The putative mitochondrial targeting sequence from the *Tfr2* gene (MERLWGLFQRAQQLSPRSSQTVYQRVEG) was subcloned by PCR from a *Tfr2* expression vector (Genecopoeia, Germantown, MD). Primers TFRmito-F (5′-CATGGTCGACGCCACCATGGAGCGGCTTTGGGGTCTA-3′) and TFRmito-R (5′-CATGGGTACCAACCCTTTCCGGGGGCCTTCCA-3′) were used to amplify the MTS and generate unique Sal I and Kpn I restriction sites on the 5′ and 3′ ends respectively of the PCR product. The PCR product was subcloned in frame into the multiple cloning site of the pDsRED-monomer (Clontech, Mountain View, CA) to generate the TfR2 MTS RFP (red fluorescent protein) vector.

Transfection of HEK 293T cells

Twenty-four hours prior to transfection, 2.25×10^5 HEK 293T cells were plated in each well of a 6 well dish. Cells were incubated for 24 h at 37 °C in a 5% CO_2 atmosphere. Prior to transfection, DNA (4 µg cyan fluorescent protein (CFP) construct + 4 µg of RFP construct) and Lipofectamine 2000 reagent (Invitrogen, Temecula,CA) were combined and incubated according to the manufacturer's recommendations. DNA/Lipofectamine 2000 mixtures were applied to cells containing 5.0 ml of serum-free DMEM. The DNA mixture was removed after 6 h of incubation and was replaced with 5.0 ml of DMEM containing 5% fetal calf serum. Transfected cells continued to grow for an additional 18 h prior to confocal microscopy analysis.

TfR2 silencing

Five clones of TfR2 silencing shRNA (Mission® shRNA, Sigma, St. Louis, MO) were purchased from Sigma. The silencing ability of each clone was assessed 24 h after transfection by western blot. The most effective clone (TRCN0000063628) – which reduced TfR2 expression by 90% – was used for all the experiments.

RT-PCR

Human tissue RNA was obtained from Ambion Inc. (Austin, TX). RT-PCR was performed using 2 µg total RNA and the SuperScript RT-PCR system (Invitrogen, Carlsbad, CA). TFR2-specific PCR was performed using two distinct primer sets (Kawabata et al., 1999).

Set A: For: 5′-GTGGTCAGTGAGGATGTCA-3′; Rev: 5′-CGTGGTCCA-GCTTCTGGCGGGAG-3′. Set B: For: 5′-ACGTCTCTGGCATCCTTCC-3′; Rev: 5′-CATCGACCCAGTGCAGGGTG-3′.

Treatment of TfR2 overexpressing cells with Alexa-conjugated transferrin

100 µg of holo-transferrin (Sigma) was labeled with the Alexa488 protein labeling kit (Molecular Probes, Eugene, OR) according to the manufacturer's instruction. HEK 293 cells overexpressing transferrin receptor 2 and mitochondrial targeted CFP (Invitrogen, Temecula, CA), were kept in serum-free medium 30 min at 37 °C, 5% CO_2, to allow cells to unload endogenous transferrin from endocytic vesicles. Then cells were incubated for 60 min at 4 °C

with labeled transferrin (3.2 nM). Cells were washed 3 times with ice-cold HBSS and then incubated again in standard cell culture medium. After 90 min, cells were stained with the potentiometric mitochondrial dye tetramethylrhodamine methyl ester TMRM (20 nM, Molecular Probes, Eugene, OR) and analyzed with an inverted laser scanning confocal microscope (Fluoview 1000, Olympus).

Release of ferrous iron (Fe^{2+}) from transferrin

Release of ferrous iron was measured as previously described (Kojima and Bates, 1979), by monitoring the absorbance of the Fe^{2+}·BPS complex (bathophenanthroline disulfonate, Sigma, St. Louis, MO) at 538 nm with a Spectramax Plus spectrophotometer (Molecular Devices, Sunnyvale, CA). BPS chelates ferrous iron exclusively and it was used 1 mM final. 1 mg of Tf of NEM-Tf was used for each reaction. The reactions were carried out in 100 mM TrisHCl pH 7.4. Xanthine was used 3 mM final, xanthine oxidase was used 0.1 U/mL. Oxidized glutathione (Sigma, St. Louis, MO) was prepared immediately before adding it to the reaction and used 7.5 mM. For all the solutions, the pH was adjusted to 7.4. Absorbance was measured after 20 min of incubation at room temperature.

At the end of each experiment, concentrated HCl was added to induce total iron release; the absorbance observed after HCl mediated ferrous release was set as 100% and used to normalize the values obtained in each experiment. Where indicated, transferrin was alkylated before the experiment with 100 mM N-ethylmaleimide (NEM) in 50 mM TrisHCl pH 6.8, room temperature. Alkylation with NEM did not result in any iron release (data not shown). Unreacted NEM was removed by microfiltration (Microcon Ultracel YM-30, Millipore, Billerica, MA). NEM modification of thiols is irreversible. To ensure alkylation of thiols,1 mg of NEM-Tf was incubated with 0.1 mM of the fluorescent thiol probe CPM, which emits only when reacted with thiol groups. While emission was detected in normal Tf, no signal was observed for NEM-Tf. Emission was measured with a microplate spectrofluorometer.

Radiolabeling of Tf

Apo-transferrin (Sigma St. Louis, MO) was labeled as previously described (Morales et al., 1987). In brief, 16 mg of apo-Tf was resuspended in 4 mL of 0.6 M NaHCO$_3$ pH 7.0 and 0.8 mL of ^{59}[Fe^{3+}] (0.8 mCi in 1% citric acid, Perkin Elmer, Waltham, MA) was added. The solution was incubated for 1 h at room temperature and excess iron was removed by size exclusion purification (Centricon 10, Millipore), according to the manufacturer's instructions. Purified labeled Tf was used at a final concentration of 3 µM in all experiments. Aqueous counting cocktail was added to the samples (Fisher Scientific, Pittsburgh, PA) and the activity was determined with a liquid scintillation spectrophotometer (Beckman Coulter, Fullerton, CA). After labeling, the activity of purified Tf was 366,868 cpm/ µg of protein.

Mitochondrial iron uptake

Iron uptake by mitochondria was measured as described by others (Zhang et al., 2005) with some modifications. In this experiment, we used HEK 293T cells transiently transfected with TfR2 or YFP; transfection efficiency was 50%–60%. Twenty-four hours after transfection, RPMI full medium was replaced with serum-free medium to allow endocytic vesicles to unload endogenous Tf. After 2 h, this medium was replaced with HBS (125 mM KCl, 2 mM K$_2$HPO$_4$, 5 mM HEPES, 5 mM MgCl$_2$, 0.02 mM EDTA, pH 7) supplemented with 3 µM radiolabeled diferric Tf. Cells were incubated for 1 h at 4 °C to allow binding of ^{59}[Fe^{3+}]$_2$-Tf to cells. After incubation, radioactive HBS was removed, cells were quickly rinsed and warm full medium was added. Cells were incubated for 2 h at 37°C in 5% CO$_2$ and then harvested with trypsin. Lysis was performed by resuspending the cells in hypotonic buffer (83 mM sucrose, 50 mM TrisHCl pH 7.4, protease inhibitor cocktail (Sigma)). After 10 min of incubation on ice, an equal volume of isotonic buffer was added (250 mM sucrose, 50 mM

TrisHCl pH 7.4, protease inhibitor cocktail (Sigma)) and cells were further disrupted in a teflon-glass homogenizer, with 50 strokes on ice. Mitochondria were isolated as described and radioactivity was measured in the mitochondrial and in the cytosolic fractions. The amount of proteins in both fractions was measured with the Bradford Coomassie method according to standard procedures (Stoscheck, 1990) and used to normalize the radioactivity counts.

Complex I iron uptake

The purpose of this experiment was to detect iron incorporation into complex I, which contains iron–sulfur clusters. To allow incorporation of iron into newly formed respiratory complexes, we used a longer incubation period to ensure cell division and, therefore, mitochondrial biogenesis. Cells overexpressing TfR2 or YFP were kept for 1 h in medium without serum as above, and then 3 h in serum-free medium supplemented with 3 µM radiolabeled Tf. After 3 h, radioactive medium was replaced with full medium and cells were further cultured for 16 h. Cells were washed with PBS, harvested and used immediately.

Complex I immunopurification

Complex I was immuno-captured as previously described (Keeney et al., 2006; Murray et al., 2003, 2004), using beads coated with an antibody specifically developed to immunoprecipitate intact complex I (MitoScience, Eugene, OR). In brief, purified mitochondria were resuspended at a final concentration of 5.5 mg/mL in PBS. Complexes were solubilized with 1% dodecyl-maltoside, incubating the solution for 30 min on ice; the solution was centrifuged for 30 min at 21,000 ×g (4 °C), and 5 µg of beads were added to the supernatant. After a 3-hour incubation at room temperature with gentle shaking, beads were washed three times with PBS, 0.01% dodecyl-maltoside. Complex I was eluted by heating the beads 10 min at 65 °C in 1% SDS, 100 mM TrisHCl pH 7.4. Radioactivity of the eluted complex was measured as above.

Cell death assay

SK-N-MC cells were transfected with the indicated vectors using the Nucleofector V kit (Amaxa, Cologne, Germany) according to the manufacturer's instructions. Transfection efficiency – which was higher than 85% – was monitored according to the manufacturer's instruction, using GFP coding vector provided in the kit. Cells were treated with rotenone (100 nM), hydrogen peroxide (1 mM) or staurosporine (1 µM). Cell death was measured as previously described, monitoring the emission of the membrane impermeable dye, Sytox green (Invitrogen, Carlsbad, CA) as previously described (Sherer et al., 2002), with minor modifications. Briefly, after treatment, cells were incubated with 1 µM Sytox for 20 min in the incubator. Emission at 523 nm – following excitation at 504 nm – was measured with a SpectraMax Gemini EM multi-plate reader (Molecular Devices, Sunnyvale, CA). After this reading, Triton X-100 was added to a final concentration of 0.1% to permeabilize the cells. After 30 min, Sytox emission was measured again; this last measurement was used to normalize the previous reading (100% cell death). Cell death was also measured in an independent set of experiments using the cell-impermeable dye, trypan blue (Invitrogen, Carlsbad, CA); positive cells were counted with a hemocytometer (Hausser Scientific, Horsham, PA).

Statistical analysis was performed using the Prism 4 software (GraphPad, SanDiego, CA); *p* values were calculated using Student *t*-test.

Results

Iron accumulation in rotenone-treated rats and monkeys

Chronic systemic administration of the complex I inhibitor, rotenone, reproduces behavioral, biochemical and neuropathological features of PD (Betarbet et al., 2006; Betarbet et al.,

2000); however, whether or not iron accumulates has not been assessed previously. Using Pearl's staining for ferric iron, we found that rotenone treatment was associated with deposition of iron within the substantia nigra, in both rat and monkeys (Fig. 1a, b). Iron accumulation was restricted to substantia nigra, and was not found in the ventral tegmental area, an adjacent dopaminergic cell group that is less vulnerable to PD pathology. Higher magnification images revealed that iron staining colocalizes with tyrosine hydroxylase positive neurons (Fig. 1a, c, d); as these iron-laden neurons developed degenerative morphological changes (e.g., vacuolar changes or shrinkage), they were often surrounded by reactive, iron-containing microglia (Fig. 1c, e). In rotenone-treated monkeys, iron could be detected within numerous neurons containing neuromelanin (Fig. 1d, panel A and Supplemental Fig. 1) and, in TH+ neurons, iron staining presented a pattern resembling mitochondria (Fig. 1d, panels B–E).

Transferrin accumulation in the rotenone model

Iron traverses cell membranes by a variety of mechanisms that may vary by organ and cell type (Connor, 1994; Rouault and Cooperman, 2006). Of these, it is generally believed that neurons use a Tf-dependent system for iron transport. To examine the potential role of Tf in nigral iron accumulation, we first studied its expression. In rotenone-treated rats and monkeys, there was a marked and selective accretion of Tf in dopaminergic neurons of the substantia nigra (Fig. 2a, b, g, h). Interestingly, as these neurons accumulated Tf, there was a tendency for loss of tyrosine hydroxylase. The immunocytochemical results showing Tf accumulation were confirmed by western blotting (Fig. 2b). Because brain Tf is thought to be synthesized and secreted primarily by oligodendroglia (Rouault and Cooperman, 2006), the observed increase in *neuronal* Tf suggests increased uptake or impaired endosomal trafficking of Tf.

Since most cellular iron is found in mitochondria (Huang et al., 2006), and because the mechanisms of neuronal mitochondrial iron accumulation are not well understood, we examined whether some of the Tf was associated with mitochondria. There is precedent for this: in erythroid cells, there is evidence that Tf-containing endosomes may transiently fuse with mitochondria to deliver iron (Ponka et al., 2002; Sheftel et al., 2007). In our experiments, we demonstrated by (i) mitochondrial subfractionation, (ii) progressive trypsinization of isolated mitochondria and (iii) electron microscopy, that a portion of the substantia nigra Tf was located in a trypsin-impermeable mitochondrial compartment, associated with the inner mitochondrial membrane (Fig. 2c–e). Consistent with these *ex vivo* results, when human neural SK-N-MC cells (which endogenously express TfR2) were treated with rotenone *in vitro*, there was accumulation of Tf and partial colocalization with the 39 kDa subunit of respiratory complex I, a mitochondrial marker (Fig. 2f). Lastly, in rotenone-treated monkeys, laser scanning confocal microscopy revealed substantial colocalization of Tf and mitochondria (Fig. 2h).

Normally, after Tf delivers its iron, it traffics back to the extracellular space (Zecca et al., 2004); as a result, intracellular Tf levels tend to remain relatively constant and low. The mechanism by which Tf accumulates after rotenone treatment is uncertain, but it is known that exposure to this complex I inhibitor causes oxidative damage to proteins, including subunits of complex I itself (Keeney et al., 2006). One of the earliest oxidative protein modifications that may occur is oxidation of thiols in cysteine residues to form intra- or inter-molecular disulfide bonds (Jones, 2006). Using a novel assay to identify oxidized thiols (Mastroberardino et al., 2008) (Supplemental Fig. 1), we found that rotenone treatment caused selective thiol oxidation in dopamine neurons of the substantia nigra in rats and in monkeys (Fig. 3a, b). Interestingly, there was generally an inverse relationship between cellular thiol oxidation and tyrosine hydroxylase levels, suggesting that oxidation causes a loss of dopaminergic phenotype prior to frank cell loss.

Oxidative modifications of Tf

Having established the presence of extensive thiol oxidation in dopamine neurons, we next assessed whether Tf undergoes an oxidative modification that might impair its trafficking. Initially, we investigated whether Tf possesses redox active thiols that can undergo oxidation depending upon the redox status of the milieu. When purified Tf was incubated in buffers of known redox potential, we observed disappearance of free thiols with increasingly oxidizing conditions (Supplemental Fig. 2). Therefore, we sought to identify which residues are susceptible to redox modification. For this purpose, we used the biotinylated thiol-reactive probe ICAT (isotope coded affinity tag) (Gygi et al., 1999) to specifically label and quantify the oxidized thiols (disulfides) in protein extracts from ventral midbrain of rotenone and control rats. ICAT is a tag that specifically modifies cysteines; it is available in two isotopic forms – heavy and light – that can be distinguished by the mass spectrometer. Therefore, ICAT provides an ideal tool to quantify thiol oxidation in proteins. Oxidized thiols were specifically labeled using a three-step procedure (Mastroberardino et al., 2008) (Supplemental Fig. 3). After trypsin digestion, the labeled peptides were avidin-purified and analyzed by mass spectrometry. We found that rotenone treatment causes a 3-fold increase in thiol oxidation at cys260 (Fig. 3e).

Consistent with the mass spectrometry result, in rotenone-treated rats we were able to demonstrate fluorescence resonance energy transfer (FRET) between our fluorescent indicator of oxidized thiols and Tf in dopamine neurons (Fig. 3d, Supplemental Fig. 1) (Mastroberardino et al., 2008). FRET occurs only when there is close proximity between the fluorophores and, therefore, indicates that the immuno-labeled protein, in this case Tf, was oxidized. Moreover, by performing SDS-PAGE and western blotting under non-reducing and reducing conditions, we showed the presence of an intermolecular disulfide bond (Fig. 3c). High molecular weight (MW) Tf immuno-reactive bands were found only in samples from rotenone-treated animals under non-reducing conditions; the high MW bands were undetectable after thiol reduction. Together, these results suggest that rotenone causes oxidative cross-linking of Tf to other proteins by the formation of a disulfide bond at cys260. Such cross-linking is likely to impair the normal trafficking of Tf.

Thiol oxidation induces reductive release of iron from Tf

Cys260 is on a loop flanking a strand that participates in iron coordination; it is quite close to the amino acid residues comprising the iron-coordination pocket, with distances ranging from 18–20 Å (Supplemental Fig. 4). The close proximity of the site of cys260 oxidation to the Fe^{3+} atom raises the possibility that as cys260 undergoes thiol oxidation, Fe^{3+} (ferric iron) is reduced to Fe^{2+} (ferrous iron). The affinity of Tf for ferrous iron is 17 orders of magnitude lower than for ferric iron, so under these circumstances, ferrous iron is expected to be released and would become available for Fenton chemistry. To assess this possibility, we directly measured the release of Fe^{2+} from purified $Tf(Fe^{3+})2$ by following the absorbance of the Fe^{2+} chelator, bathophenanthroline disulfonate, under various conditions *in vitro*. Initially, we determined whether production of ROS *per se* could induce the release of ferrous iron from Tf. For this purpose, we incubated $Tf(Fe^{3+})_2$ with the ROS generating system xanthine/ xanthine oxidase. ROS caused release of ferrous iron and, importantly, this effect was inhibited when free thiols were made unavailable by prior alkylationwith N-ethyl-maleimide, thus indicating a role for cysteines in the Fe^{2+} release process (Fig. 3f).

We therefore explored the possibility that the formation of mixed disulfides could cause release of ferrous iron as well. Indeed, incubation of $Tf(Fe^{3+})_2$ with GSSG to create a mixed disulfide caused a *reductive* release of Fe^{2+} from $Tf(Fe^{3+})_2$, consistent with our hypothesis (Fig. 3f). If the thiols of $Tf(Fe^{3+})_2$ were made unavailable by prior alkylation with N-ethyl-maleimide, GSSG release of Fe^{2+} was greatly reduced. Thus, thiol oxidation of $Tf(Fe^{3+})_2$ is able to induce release of ferrous iron. In summary, cys260 oxidation may be responsible for both the

accumulation of Tf and the reductive release of its iron. Why Tf is associated with mitochondria, however, remained to be determined.

Transferrin receptor 2 is localized in mitochondria in dopaminergic neurons

Tf crosses the plasma membrane by endocytosis after binding to a Tf receptor (Rouault and Cooperman, 2006). Initial screening of the distribution of the predominant Tf receptor, transferrin receptor 1 (TfR1), showed relatively little protein expression in substantia nigra dopaminergic neurons compared to neurons in other regions (Supplemental Fig. 6). In contrast, immunocytochemistry using several different mono- and polyclonal antibodies revealed that there was heavy and selective expression of TfR2 protein in dopaminergic neurons (Fig. 4a). Adjacent neurons in the substantia nigra pars reticulata had low to no expression of TfR2 (Fig. 4a, b), and surrounding astrocytes and microglia had none (not shown).

As noted, in erythroid cells, Tf may participate in the delivery of iron to mitochondria; however, there has never been a demonstration of TfRs in or on mitochondria. To determine whether TfR2, like Tf, was also localized in mitochondria, we performed mitochondrial sub-fractionation, progressive trypsinization of isolated mitochondria and electron microscopy, all of which showed the presence of TfR2 in mitochondria (Fig. 2e–f).

A common way in which nuclear-encoded proteins are targeted to mitochondria is by means of an N-terminal mitochondrial targeting sequence (MTS) (Neupert and Herrmann, 2007). Analysis of the amino acid sequence of the transmembrane domains of the TfRs using two different software programs, TargetP (Emanuelsson et al., 2000) and iPSORT (Bannai et al., 2002), assigned a putative mitochondrial localization to TrfR2, but not to TfR1. To confirm that this TfR2 sequence would target a protein to mitochondria, we co-transfected cells with (i) cyan fluorescent protein (CFP) containing a known MTS (from cytochrome c oxidase) and (ii) wild-type red fluorescent protein (RFP), or RFP engineered to contain the putative MTS from TfR2.

As expected, normal RFP had a diffuse distribution in the cell and there was no colocalization with mitochondria (Fig. 5a). Conversely, RFP containing the putative TfR2 MTS was heavily colocalized with mitochondria, and there was relatively little cytoplasmic RFP (Fig. 5a). In summary, within substantia nigra as a whole, TfR2 is heavily localized to mitochondria in dopaminergic neurons.

In dopamine neurons from control animals, there was relatively little expression of Tf and TfR2, but there was substantial colocalization – and we were able to demonstrate FRET between the 2 proteins, indicating a physical interaction (molecular proximity) of the proteins (Fig. 5b) (Kenworthy, 2001). After rotenone treatment, there was an increase in the levels of both proteins and the amount of FRET between them also increased (Fig. 5b).

The Tf-TfR2 system mediates Tf and iron transport into mitochondria

To assess the functional role of the Tf-TfR2 system, cells were transiently co-transfected with wild-type TfR2 and CFP containing a consensus MTS; the cells were also labeled with the mitochondrial potentiometric dye, TMRM. Cells were then exposed to exogenous extracellular $Tf(Fe^{3+})_2$, which was labeled with Alexa488. In this experiment, the mitochondria of all cells (transfected or not) were visualized with TMRM, and transfected cells were identified by their expression of CFP-MTS.

In untransfected cells, 90 min after exposure to fluorescently labeled Tf, there was only a relatively small amount of Tf visualized and it was localized in small puncta that did not overlap with TMRM-labeled mitochondria (Fig. 6a, arrow-heads). In stark contrast, cells expressing

TfR2 were labeled intensely with Tf and most of the Tf signal was contained within mitochondria (Fig. 6a, arrows).

To confirm that iron is transported into mitochondria along with Tf, we loaded apo-Tf with $^{59}[Fe^{3+}]$ and then incubated it with cells that were transiently transfected with TfR2. In the first experiment, 2 h after this incubation, mitochondria were isolated and $^{59}[Fe^{3+}]$ was detected by liquid scintillation counting. Exogenous expression of TfR2 (with about 50% transfection efficiency) was associated with a 6-fold increase in mitochondrial iron uptake, and a smaller increase in cytosolic uptake (Fig. 6b); this effect was blocked by co-expression of a shRNA directed against TfR2. To determine whether some of this iron was being incorporated into any of the many mitochondrial proteins that contain Fe–S clusters, we performed a second experiment in which, 16 h after incubation, complex I (composed of 46 protein subunits and 8 Fe–S clusters) was immunoprecipitated from isolated mitochondria and assessed for $^{59}[Fe^{3+}]$ incorporation. In these dividing cells, which are undergoing mitochondrial biogenesis, TfR2 expression enhanced the uptake of $^{59}[Fe^{3+}]$ into complex I (Fig. 6b). Under the conditions of this experiment, about 10% of the iron transported into mitochondria was found in complex I; the remaining iron was presumably incorporated into other Fe–S cluster- or heme-containing proteins. These results indicate that the Tf-TfR2 system mediates uptake of Tf and iron into mitochondria, and this iron can be incorporated into mitochondrial proteins.

Fe–S clusters are particularly sensitive to oxidative modification and disulfide formation (Gardner and Fridovich, 1991; Taylor et al., 2003). The increase of Tf/TfR2-mediated iron import – which is seen after rotenone treatment *in vivo* (Fig. 5b) – might be a compensatory, protective response, possibly an attempt to replace damaged Fe–S clusters. Consistent with this possibility, overexpression of TfR2 in neuroblastoma cells exposed to rotenone was neuroprotective – and this effect was reversed by a shRNA directed against TfR2 which effectively reduces protein expression (Fig. 6d). Interestingly, TfR2 overexpression did not protect against H_2O_2 or staurosporine. This suggests that TfR2 protects against insults that specifically induce mitochondrial oxidative stress (i.e. rotenone), but not necessarily against generalized oxidative stress or other insults.

The Tf-TfR2 system in human Parkinson's disease

RT-PCR demonstrated the presence of TfR2 transcript in whole brain and in substantia nigra human cDNA libraries (Supplemental Fig. 7). In the normal human substantia nigra, TfR2 protein was found selectively in dopaminergic neurons, and it was colocalized, in large part, with mitochondria (Fig. 7a). In the substantia nigra of individuals who died with PD, average TH immunoreactivity was reduced in surviving dopamine neurons ($p<0.05$) and there was a dramatic increase in Tf immunoreactivity in the same neurons and in the surrounding neuropil ($p<0.001$; Fig. 7b, c). In PD cases, part of the Tf colocalized with mitochondria (Fig. 7e). Additionally, as in rotenone-treated animals, FRET revealed the presence of excess thiol oxidation of Tf in dopaminergic neurons from PD cases compared to controls (Fig. 7d). Thus, both Tf and TfR2 are present in human substantia nigra, and in PD, oxidized Tf accumulates in dopaminergic neurons, as predicted by the rotenone model.

Discussion

While iron accumulation has been recognized as a pathological feature of PD for over 80 years, the mechanism of this process has not been described. Similarly, how iron is transported into mitochondria has been unclear and may vary by cell type. The novel system we have described is unique in several respects. First, it appears to bypass the cytosolic (non-Tf-bound) iron pool, which is conventionally thought to be the main source of iron for mitochondria (Rouault and Cooperman, 2006). Second, there is direct trafficking of Tf into mitochondria, a phenomenon not reported previously. Third, this system involves TfR2, whose function is not well

understood, but which is clearly distinct from TfR1 (Trinder and Baker, 2003). Fourth, we discovered that TfR2 is targeted to mitochondria by a previously unrecognized MTS. Finally, this Tf/TfR2-dependent system is disrupted in PD and models thereof, and this appears to be a mechanism of iron accumulation in this disorder.

Mitochondrial iron transport

According to current thinking (Rouault and Cooperman, 2006), extracellular iron-bound transferrin (diferric Tf or holo-Tf) binds to TfR1 on the plasma membrane and this complex undergoes endocytosis. It is believed that the acidic environment of the endosome causes iron to dissociate from Tf, and the free iron is then reduced by endosomal reductases and extruded into the cytosol by divalent metal transporter-1 (DMT1). From there, it is unclear how iron enters mitochondria. An alternative mechanism described in immature erythroid cells proposes a transient physical association ("kiss and run") between endosomes and mitochondria (Ponka et al., 2002; Sheftel et al., 2007). These studies provide several lines of evidence for a direct interaction between transferrin-containing vesicles and mitochondria.

Additionally, the authors suggest that iron derived from Tf-containing vesicles can reach the inner mitochondrial membrane without entering the cytosolic, chelatable iron pool. Even in this scenario, however, it is assumed that iron dissociates from Tf in the endosome and that Tf plays no direct role in transporting iron into mitochondria. Following iron release, Tf traffics back to the extracellular space.

Transferrin

In this study, we found that in cells expressing TfR2, diferric Tf is directed into mitochondria, where it releases its iron for incorporation into the Fe–S clusters of complex I. In the setting of PD and the rotenone model of PD, Tf accumulates in dopaminergic neurons and some of it becomes oxidized at cys260. As noted, this thiol residue is located near the iron-coordination pocket, and we have shown in an *in vitro* system that oxidation of thiols to disulfide bonds is associated with reduction of Fe^{3+} (ferric iron) to Fe^{2+} (ferrous iron). Because the affinity of Tf for ferrous iron is 17 orders of magnitude lower than for ferric iron, ferrous iron is released.

In the *in vivo* setting, this Fe^{2+} likely becomes available for Fenton chemistry — with generation of the highly reactive and cytotoxic hydroxyl radical. Furthermore, because the oxidation of cys260 results in formation of an *intermolecular* disulfide bond, there is likely to be a conformational change in the iron-bound Tf, which might also reduce its affinity for iron and lead to deposition of iron (Baker et al., 2003). Interestingly, cys260 is relatively close to gly277, mutation of which (G277S), has been associated with increased risk for PD (this polymorphism has been also termed G258S, according to the nomenclature in another paper (Hershberger et al., 1991)). In this study, the authors suggested that the mutation could promote conformational alterations and facilitate iron release.

Normally, after iron is released from Tf and exported from the endosome, endosomal Tf is recycled back to the extracellular space (Zecca et al., 2004); however, in the rotenone model and in PD, there is massive accumulation of intracellular Tf. Whether this is due to enhanced uptake of Tf, impaired recycling of endosomal Tf, or some combination of the two is uncertain. Our finding that Tf is bound to other proteins via an intermolecular disulfide bond suggests that Tf may become 'anchored' to other cellular constituents, rendering it unavailable for normal recycling.

Transferrin receptor 2

TfR2 shares about 45% homology with TfR1, but its function in iron homeostasis remains elusive (Kawabata et al., 1999). Unlike TfR1, TfR2 mRNA does not contain an iron responsive

element, and is therefore not regulated by iron levels (Trinder and Baker, 2003). It has a lower affinity and higher capacity for Tf binding than TfR1, and in cells in which the *TfR1* gene has been silenced, TfR2 cannot replace its function (Trinder and Baker, 2003). Interestingly, there is evidence that TfR2 levels may be regulated by levels of diferric Tf; as Tf increases, so does TfR2 (Johnson and Enns, 2004). Thus, the increased TfR2 levels we have found in dopamine neurons might, in part, be secondary to Tf accumulation. It has also been suggested that hepatocyte TfR2 may function as an 'iron sensor', in essence, measuring plasma iron content (Ganz, 2004). Mutations of TfR2 are a rare cause the severe systemic iron overload disease, hereditary hemochromatosis (Camaschella et al., 2000).

Although there have been relatively few studies on the subcellular distribution of TfR2, in general, it has been associated with the plasma membrane and with endosomes (Johnson et al., 2006; Merle et al., 2007). In this study, we have provided compelling evidence that in dopamine neurons, TfR2 is localized, in part, to mitochondria. Moreover, when cells express exogenous TfR2, extracellular diferric Tf is rapidly taken up and transported to mitochondria. Thus, this Tf/ TfR2 system appears to represent a major mechanism for iron transport into mitochondria of certain neuronal populations.

Parkinson's disease

The importance of iron deposition in the pathogenesis of PD has been unclear; however, epidemiological and genetic evidence suggests that elevated iron levels or abnormal iron homeostasis may increase the relative risk of developing PD. For example, increased dietary iron or red meat consumption is associated with a higher risk of PD (Powers et al., 2003). As noted, a polymorphism in Tf is associated with increased risk of PD (Borie et al., 2002). Similarly, mutations in the predominant hemochromatosis gene, *HFE*, have recently been proposed as a risk factor for PD (Dekker et al., 2003; Guerreiro et al., 2006). Together, epidemiological and genetic studies suggest that abnormalities in iron homeostasis may predispose to PD. Experimental data also support this conclusion. Chelation of iron by pharmacological or genetic means protects dopamine neurons from toxins that induce dopaminergic degeneration (Ben-Shachar et al.,1991; Kaur et al., 2003). Furthermore, postnatal dietary supplementation with high amounts of iron sensitizes mice to a toxin that induces parkinsonism (Kaur et al., 2006).

In PD, the initial cellular source of iron deposition in substantia nigra is unknown. Most commonly, iron seems to be associated with activated microglia, which are often seen surrounding remnants of degenerating dopamine neurons, such as extracellular Lewy bodies or neuromelanin (Jellinger et al., 1990). Less commonly, iron is also seen in substantia nigra neurons in a diffuse pattern (Jellinger et al., 1990; Morris et al., 1992); however, it has recently been demonstrated for the first time that iron levels are elevated in individual dopaminergic neurons in PD (Oakley et al., 2007). Consistent with this, our studies in rotenone-treated rats and monkeys suggest that iron initially accumulates in neurons, and then as the neurons undergo degenerative changes, they are engulfed by microglia, whereupon iron appears in a punctate distribution in these cells. In rotenone-treated monkeys, we identified dopaminergic (tyrosine hydroxylase immunoreactive) neurons with intense iron labeling. In the rat, although substantia nigra neurons containing iron did not contain tyrosine hydroxylase immunoreactivity, there are several reasons to believe they are also dopaminergic. First, we have demonstrated that Tf accumulates selectively in dopamine neurons. Second, within substantia nigra, TfR2 is localized selectively in the dopamine neurons; nearby GABAergic neurons and surrounding astrocytes and microglia do not express the receptor. Third, as neurons accumulate oxidative damage and Tf, they tend to lose tyrosine hydroxylase immunoreactivity.

As noted, although Tf and TfR2 accumulate identically in rotenone-treated rats and monkeys, *iron-laden* dopamine neurons are only seen unequivocally in monkeys. The reasons for the

inter-species differences in the observed iron phenotype need to be investigated in more depth. Monkeys, like humans, have neuromelanin in their substantia nigra dopaminergic neurons (Fig. 1b, Fig. 7b), but rats do not. This pigment binds iron, and has been suggested to play a protective role (Li et al., 2005;Zecca et al., 2006). This intrinsic iron buffering mechanism may permit primate neurons to tolerate higher total iron concentrations, which can then be detected within the sensitivity range of the Perl's iron stain. In contrast, in the absence of this iron buffering, the same iron levels may be toxic to rat neurons and, by the time iron reaches levels that are detectable by Perl's staining, the cells lose their TH phenotype and die. At that stage, iron would be detected mostly in the microglia. In conclusion, we believe that degenerating dopaminergic neurons are the initial cellular source of iron in PD.

Accumulation of iron may have particularly dire consequences in dopaminergic neurons because dopamine metabolism generates substantial H_2O_2. Ferrous iron reacts with H_2O_2 via Fenton chemistry to generate the highly reactive and cytotoxic hydroxyl radical. Thus, iron may contribute to the oxidative damage that characterizes PD. In addition, elevated iron may play a role in the accumulation of α-synuclein in dopaminergic neurons in PD and the rotenone model thereof. Indeed, it has recently been reported that the 5′-UTR in the mRNA encoding α-synuclein contains a putative iron responsive element (Friedlich et al., 2007). Therefore, increased iron may lead to a post-transcriptional up-regulation of a-synuclein protein.

Why does iron increase in PD?

Having established a plausible mechanism of how iron accumulates in PD, perhaps the most important question is *why* iron accumulates. It has been suggested that a mitochondrial Fe–S cluster-containing protein may act as a 'sensor' of mitochondrial iron status (Rouault and Tong, 2005). Such proteins are extraordinarily sensitive to attack by superoxide (Gardner and Fridovich, 1991), which is generated by complex I dysfunction in the rotenone model (Panov et al., 2005), and probably in PD. It is known that subunits of complex I are oxidatively damaged in PD and that this pattern of damage can be reproduced by exposure to rotenone (Keeney et al., 2006). Whether or not the specific subunits that contain Fe–S clusters are damaged is not known, but we have previously presented evidence that this is the case (Panov et al., 2005). Given our results showing that rotenone induces superoxide production and early thiol oxidation, we hypothesize that Fe–S clusters may be oxidized in PD and by rotenone. If so, they would be unable to bind iron properly. With ongoing oxidative stress, there would be a continuous signal to replace the damaged Fe–S clusters but an inability to properly insert the iron. In essence, there would be an unopposed signal to bring in more iron but no way to properly utilize it. This possibility is currently under investigation.

In summary, we have described a novel Tf/TfR2-dependent system for iron transport into neuronal mitochondria. The extent to which this system participates in mitochondrial iron transport in other cell types and organs remains to be determined. We have provided evidence that in Parkinson's disease, there is disruption of this pathway (Fig. 7), which leads to iron deposition in substantia nigra. Because iron participates in Fenton chemistry to generate cytotoxic hydroxyl radicals, it is likely that it contributes importantly to the pathogenesis of PD. Further studies will evaluate if transferrin accumulation and oxidation constitute a reliable, potential biomarker to monitor oxidative stress as well as the progression of the pathogenesis in PD. Additionally the Tf/TfR pathway has been proposed as a means to deliver therapeutics into the brain, through the blood brain barrier (Pardridge, 2007;Qian et al., 2002). Hence, the increased transport of Tf in dopaminergic neurons might constitute the basis for an appealing, specific drug delivery strategy. As such, this pathway may represent a therapeutic target to slow the progression of this devastating neurodegenerative disorder, and perhaps others that are likewise associated with iron accumulation.

Supplementary Material

Refer to Web version on PubMed Central for supplementary material.

Acknowledgments

Appendix A Supplementary data

Supplementary data associated with this article can be found, in the online version, at doi: 10.1016/j.nbd.2009.02.009.

References

Baker HM, et al. Dealing with iron: common structural principles in proteins that transport iron and heme. Proc. Natl. Acad. Sci. U. S. A 2003;100:3579–3583. [PubMed: 12642662]

Bannai H, et al. Extensive feature detection of N-terminal protein sorting signals. Bioinformatics 2002;18:298–305. [PubMed: 11847077]

Ben-Shachar D, et al. The iron chelator desferrioxamine (Desferal) retards 6-hydroxydopamine-induced degeneration of nigrostriatal dopamine neurons. J. Neurochem 1991;56:1441–1444. [PubMed: 1900527]

Berg D, Hochstrasser H. Iron metabolism in parkinsonian syndromes. Mov. Disord 2006;21:1299–1310. [PubMed: 16817199]

Betarbet R, et al. Intersecting pathways to neurodegeneration in Parkinson's disease: effects of the pesticide rotenone on DJ-1, alpha-synuclein, and the ubiquitin-proteasome system. Neurobiol. Dis 2006;22:404–420. [PubMed: 16439141]

Betarbet R, et al. Chronic systemic pesticide exposure reproduces features of Parkinson's disease. Nat. Neurosci 2000;3:1301–1306. [PubMed: 11100151]

Borie C, et al. Association study between iron-related genes polymorphisms and Parkinson's disease. J. Neurol 2002;249:801–804. [PubMed: 12140659]

Camaschella C, et al. The gene *TFR2* is mutated in a new type of haemochromatosis mapping to 7q22. Nat. Genet 2000;25:14–15. [PubMed: 10802645]

Campuzano V, et al. Friedreich's ataxia: autosomal recessive disease caused by an intronic GAA triplet repeat expansion. Science 1996;271:1423–1427. [PubMed: 8596916]

Choo YS, et al. Mutant huntingtin directly increases susceptibility of mitochondria to the calcium-induced permeability transition and cytochrome *c* release. Hum. Mol. Genet 2004;13:1407–1420. [PubMed: 15163634]

Connor JR. Iron regulation in the brain at the cell and molecular level. Adv. Exp. Med. Biol 1994;356:229–238. [PubMed: 7887227]

Curtis AR, et al. Mutation in the gene encoding ferritin light polypeptide causes dominant adult-onset basal ganglia disease. Nat. Genet 2001;28:350–354. [PubMed: 11438811]

Dekker MC, et al. Mutations in the hemochromatosis gene (*HFE*), Parkinson's disease and parkinsonism. Neurosci. Lett 2003;348:117–119. [PubMed: 12902032]

Emanuelsson O, et al. Predicting subcellular localization of proteins based on their N-terminal amino acid sequence. J. Mol. Biol 2000;300:1005–1016. [PubMed: 10891285]

Friedlich AL, et al. The 5′-untranslated region of Parkinson's disease alpha-synuclein messengerRNA contains a predicted iron responsive element. Mol. Psychiatry 2007;12:222–223. [PubMed: 17325711]

Ganz T. Is TfR2 the iron sensor? Blood 2004:3839–3840.

Gardner PR, Fridovich I. Superoxide sensitivity of the *Escherichia coli* aconitase. J. Biol. Chem 1991;266:19328–19333. [PubMed: 1655783]

Gotz ME, et al. The relevance of iron in the pathogenesis of Parkinson's disease. Ann. N. Y. Acad. Sci 2004;1012:193–208. [PubMed: 15105267]

Greenamyre JT, Hastings TG. Biomedicine. Parkinson's—divergent causes, convergent mechanisms. Science 2004;304:1120–1122. [PubMed: 15155938]

Guerreiro RJ, et al. Association of HFE common mutations with Parkinson's disease, Alzheimer's disease and mild cognitive impairment in a Portuguese cohort. BMC Neurol 2006;6:24. [PubMed: 16824219]

Gutekunst CA, et al. Nuclear and neuropil aggregates in Huntington's disease: relationship to neuropathology. J. Neurosci 1999;19:2522–2534. [PubMed: 10087066]

Gygi SP, et al. Quantitative analysis of complex protein mixtures using isotope-coded affinity tags. Nat. Biotechnol 1999;17:994–999. [PubMed: 10504701]

Halliwell, B.; Gutteridge, JMC. Oxford: Oxford University Press; 1999. Free Radicals in Biology and Medicine.

Hatefi Y. The mitochondrial electron transport and oxidative phosphorylation system. Annu. Rev. Biochem 1985;54:1015–1069. [PubMed: 2862839]

Hershberger CL, et al. A cloned gene for human transferrin. Ann. N. Y. Acad. Sci 1991;646:140–154. [PubMed: 1809186]

Hovius R, et al. Improved methods to isolate and subfractionate rat liver mitochondria Lipid composition of the inner and outer membrane. Biochim. Biophys. Acta 1990;1021:217–226. [PubMed: 2154259]

Huang XP, et al. Mitochondrial involvement in genetically determined transition metal toxicity I. Iron toxicity. Chem. Biol. Interact 2006;163:68–76. [PubMed: 16797509]

Iversen SD, Iversen LL. Dopamine: 50 years in perspective. Trends Neurosci 2007;30:188–193. [PubMed: 17368565]

Jellinger K, et al. Brain iron and ferritin in Parkinson's and Alzheimer's diseases. J. Neural. Transm. Park. Dis. Dement. Sect 1990;2:327–340. [PubMed: 2078310]

Johnson MB, et al. Transferrin receptor 2: evidence for ligand-induced stabilization and redirection to a recycling pathway. Mol. Biol. Cell 2006;18:743–754. [PubMed: 17182845]

Johnson MB, Enns CA. Diferric transferrin regulates transferrin receptor 2 protein stability. Blood 2004;104:4287–4293. [PubMed: 15319290]

Jones DP. Redefining oxidative stress. Antioxid. Redox Signal 2006;8:1865–1879. [PubMed: 16987039]

Kaur D, et al. Increased murine neonatal iron intake results in Parkinson-like neurodegeneration with age. Neurobiol. Aging 2006;28:907–913. [PubMed: 16765489]

Kaur D, et al. Genetic or pharmacological iron chelation prevents MPTP-induced neurotoxicity in vivo: a novel therapy for Parkinson's disease. Neuron 2003;37:899–909. [PubMed: 12670420]

Kawabata H, et al. Molecular cloning of transferrin receptor 2. A new member of the transferrin receptor-like family. J. Biol. Chem 1999;274:20826–20832.

Keeney PM, et al. Parkinson's disease brain mitochondrial complex I has oxidatively damaged subunits and is functionally impaired and misassembled. J. Neurosci 2006;26:5256–5264. [PubMed: 16687518]

Kenworthy AK. Imaging protein-protein interactions using fluorescence resonance energy transfer microscopy. Methods 2001;24:289–296. [PubMed: 11403577]

Kojima N, Bates GW. The reduction and release of iron from Fe3+·transferrin·CO3(2—). J. Biol. Chem 1979;254:8847–8854. [PubMed: 479164]

Li J, et al. Differential effects of human neuromelanin and synthetic dopamine melanin on neuronal and glial cells. J. Neurochem 2005;95:599–608. [PubMed: 16135091]

Liao L, et al. Proteomic characterization of postmortem amyloid plaques isolated by laser capture microdissection. J. Biol. Chem 2004;279:37061–37068. [PubMed: 15220353]

Mastroberardino PG, et al. A FRET-based method to study protein thiol oxidation in histological preparations. Free Radic. Biol. Med 2008;45:971–981. [PubMed: 18620047]

Merle U, et al. Localization of the iron-regulatory proteins hemojuvelin and transferrin receptor 2 to the basolateral membrane domain of hepatocytes. Histochem. Cell Biol 2007;127:221–226. [PubMed: 16932966]

Morales C, et al. Transport of iron and transferrin synthesis by the seminiferous epithelium of the rat in vivo. Biol. Reprod 1987;37:995–1005. [PubMed: 3689862]

Morris CM, et al. Histochemical distribution of non-haem iron in the human brain. Acta Anat. (Basel) 1992;144:235–257. [PubMed: 1529678]

Murray J, et al. The subunit composition of the human NADH dehydrogenase obtained by rapid one-step immunopurification. J. Biol. Chem 2003;278:13619–13622. [PubMed: 12611891]

Murray J, et al. Focused proteomics: towards a high throughput monoclonal antibody-based resolution of proteins for diagnosis of mitochondrial diseases. Biochim. Biophys. Acta 2004;1659:206–211. [PubMed: 15576053]

Neupert W, Herrmann JM. Translocation of proteins into mitochondria. Annu. Rev. Biochem. 2007

Oakley AE, et al. Individual dopaminergic neurons show raised iron levels in Parkinson disease. Neurology 2007;68:1820–1825. [PubMed: 17515544]

Panov A, et al. Rotenone model of Parkinson disease: multiple brain mitochondria dysfunctions after short term systemic rotenone intoxication. J. Biol. Chem 2005;280:42026–42035. [PubMed: 16243845]

Panov AV, et al. Early mitochondrial calcium defects in Huntington's disease are a direct effect of polyglutamines. Nat. Neurosci 2002;5:731–736. [PubMed: 12089530]

Pardridge WM. Drug targeting to the brain. Pharm. Res 2007;24:1733–1744. [PubMed: 17554607]

Ponka P, et al. Iron targeting to mitochondria in erythroid cells. Biochem. Soc. Trans 2002;30:735–738. [PubMed: 12196181]

Powers KM, et al. Parkinson's disease risks associated with dietary iron, manganese, and other nutrient intakes. Neurology 2003;60:1761–1766. [PubMed: 12796527]

Przedborski S, et al. The parkinsonian toxin 1-methyl-4-phenyl-1,2,3,6-tetrahydropyridine (MPTP): a technical review of its utility and safety. J.Neurochem 2001;76:1265–1274. [PubMed: 11238711]

Qian ZM, et al. Targeted drug delivery via the transferrin receptor-mediated endocytosis pathway. Pharmacol. Rev 2002;54:561–587. [PubMed: 12429868]

Rouault TA, Cooperman S. Brain iron metabolism. Semin. Pediatr. Neurol 2006;13:142–148. [PubMed: 17101452]

Rouault TA, Tong WH. Iron-sulphur cluster biogenesis and mitochondrial iron homeostasis. Nat. Rev. Mol. Cell Biol 2005;6:345–351. [PubMed: 15803140]

Sheftel AD, et al. Direct interorganellar transfer of iron from endosome to mitochondrion. Blood 2007;110:125–132. [PubMed: 17376890]

Sherer TB, et al. An in vitro model of Parkinson's disease: linking mitochondrial impairment to altered alpha-synuclein metabolism and oxidative damage. J. Neurosci 2002;22:7006–7015. [PubMed: 12177198]

Smith MA, et al. Iron accumulation in Alzheimer disease is a source of redox-generated free radicals. Proc. Natl. Acad. Sci. U. S. A 1997;94:9866–9868. [PubMed: 9275217]

Stoscheck CM. Increased uniformity in the response of the Coomassie blue G protein assay to different proteins. Anal. Biochem 1990;184:111–116. [PubMed: 2321747]

Taylor ER, et al. Reversible glutathionylation of complex I increases mitochondrial superoxide formation. J. Biol. Chem 2003;278:19603–19610. [PubMed: 12649289]

Trinder D, Baker E. Transferrin receptor 2: a new molecule in iron metabolism. Int. J. Biochem. Cell Biol 2003;35:292–296. [PubMed: 12531241]

Watson WH, et al. Redox potential of human thioredoxin 1 and identification of a second dithiol/disulfide motif. J. Biol. Chem 2003;278:33408–33415. [PubMed: 12816947]

Zecca L, et al. Iron, brain ageing and neurodegenerative disorders. Nat. Rev. Neurosci 2004;5:863–873. [PubMed: 15496864]

Zecca L, et al. A proposed dual role of neuromelanin in the pathogenesis of Parkinson's disease. Neurology 2006;67:S8–S11. [PubMed: 17030740]

Zhang AS, et al. Intracellular kinetics of iron in reticulocytes: evidence for endosome involvement in iron targeting to mitochondria. Blood 2005;105:368–375. [PubMed: 15331447]

Zhou B, et al. A novel pantothenate kinase gene (*PANK2*) is defective in Hallervorden-Spatz syndrome. Nat. Genet 2001;28:345–349. [PubMed: 11479594]
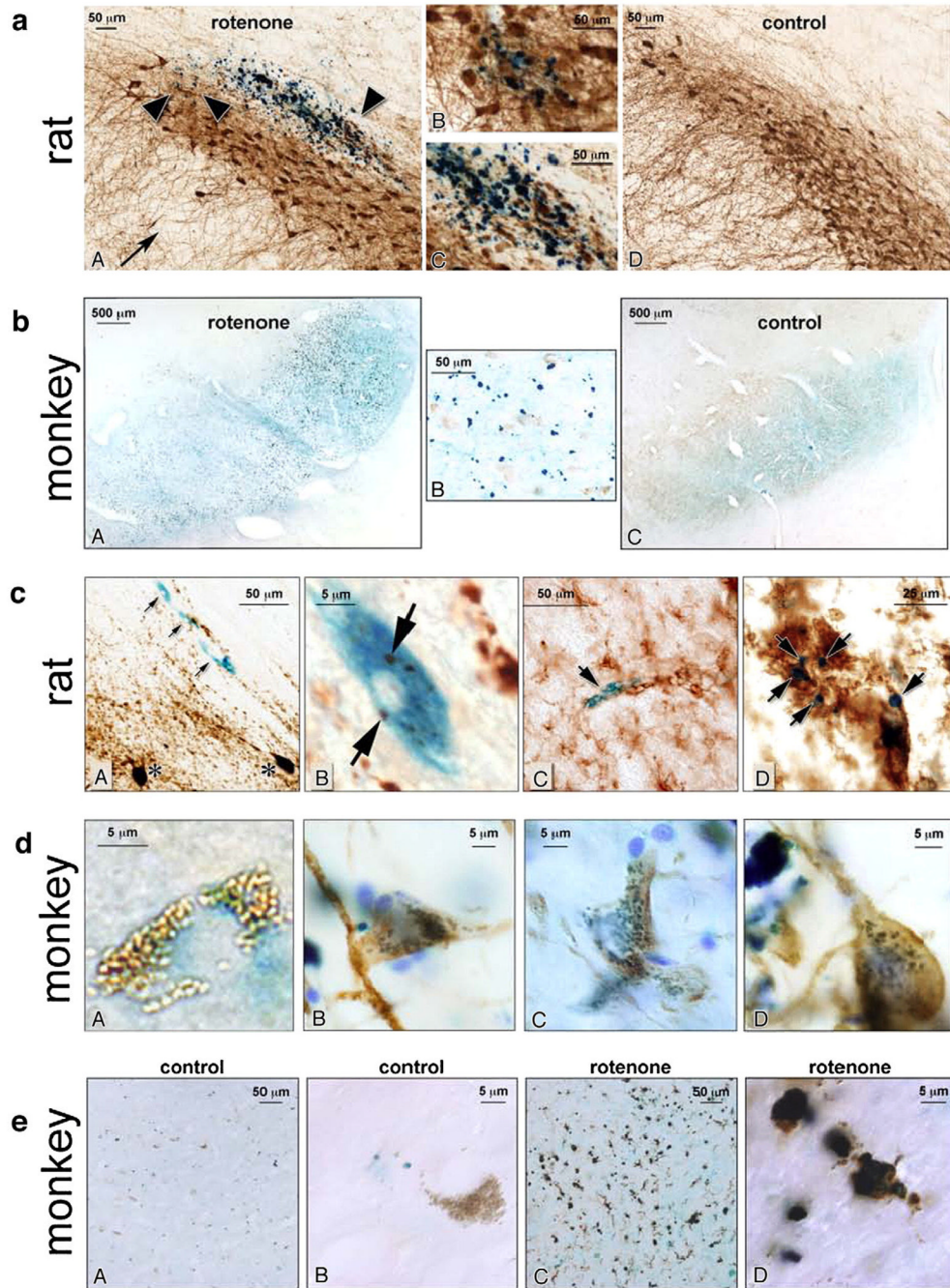
Fig. 1.
(a) Iron deposition in substantia nigra of rotenone-treated (A) and control rats (D) (20×). Iron deposits are indicated by dark blue reaction product (arrow-heads in panel A mark iron deposits; arrow shows dendritic arborization of dopamine neurons, with moderate loss of processes after rotenone treatment). The two central panels B, C are higher magnification images (40×) showing co-localization of the iron deposits and TH+ neurons. (b) Iron deposition in the substantia nigra of rotenone-treated (A) and control (C) monkeys (5×). Neuromelanin-containing neurons have light brown appearance. The central panel B is a higher magnification detail (40×) of a rotenone-treated monkey brain, where iron deposits can be seen inside and outside the neuromelanin containing neurons. (c) Colocalization of iron in both neurons and

microglia. Panel A (40×) shows iron deposition within neuronal profiles (arrows) in a rotenone-treated rat. The section was also labeled for tyrosine hydroxylase (brown)as a maker for dopamine neurons. Although the iron-laden neurons do not stain for tyrosine hydroxylase, they are approximately the same size as the nearby dopamine neurons, indicated by asterisks. Panel B shows a higher magnification (100×) of an iron-laden neuron. Note the TH associated chromogen deposits (arrows).In panel C (40×),a degenerating iron-laden blue neuronal profile is shown (arrow). The degenerating neuron is surrounded by activated microglia (brown), which were identified by OX-42 immunoreactivity. At a later stage (panel D, 60×), punctate iron (arrows) is seen within a cluster of reactive microglia. (d) Panel A shows a high magnification image (100×) of a substantia nigra monkey neuron containing neuromelanin (brown) with diffuse iron deposition (blue). In panels B–D (100×), tyrosine hydroxylase positive neurons (brown) show blue iron deposition in a mitochondrial-like punctate pattern. (e) Iron deposits in microglia in monkey tissue (A, C 20×; B, D 100×). Tissue was stained for iron (blue) and microglia (brown) using an anti-CD68 antibody. Panels A and B show low- and high-power views, respectively, of iron and microglia in a control animal; note the melanized neuron in B. Panels C and D show iron and microglia in a rotenone-treated animal. There is activation of microglia and many of the microglia contain large iron deposits.
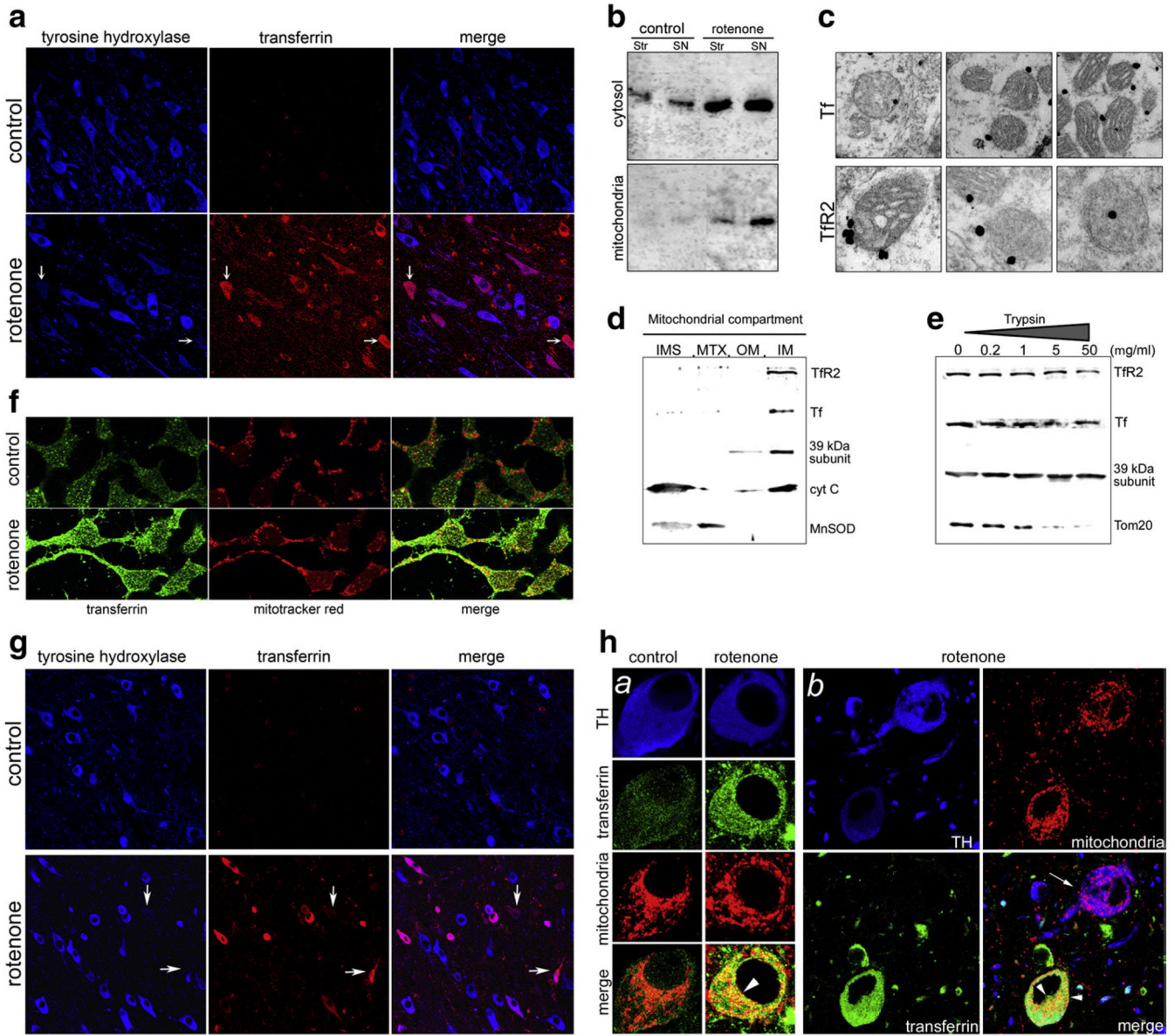
Fig. 2.
(a) Rotenone treatment induces a selective increase in Tf in rat dopaminergic neurons. Those neurons with the greatest amount of Tf accumulation (arrows) tend to have the greatest loss of tyrosine hydroxylase (TH) immunoreactivity. (b) Immunoblotting of Tf in striatal and substantia nigra cytosolic and mitochondrial fractions from control and rotenone-treated rats. With rotenone treatment, there was a marked increase in Tf, particularly in mitochondria from substantia nigra (mitochondrial marker=39 kDa subunit of the respiratory complex I). (c) Immuno-electron microscopy shows that both Tf (top row) and TfR2 (bottom row) are associated with substantia nigra mitochondria. (d) Subfractionation of mitochondria reveals Tf and TfR2 associated with the inner mitochondrial membrane (IM) along with the 39 kDa subunit of complex I. As expected, cytochrome *c* (cyt *C*) is associated with both the IM and the intermembrane space (IMS); Mn-superoxide dismutase (MnSOD) is found in matrix (MTX) and, to a lesser extent, in the IMS. (e) Progressive trypsinization of isolated mitochondria shows that Tf and TfR2 are located in a trypsin resistant compartment, like the

inner membrane protein, the 39 kDa subunit of complex I. In contrast, an outer membrane protein, Tom20, is digested by moderate concentrations of trypsin. (f) In human SK-N-MC neural cells, rotenone (50 nM for 3 days) induced an increase in Tf and colocalization with a mitochondrial marker. (g) Similar to rotenone-treated rats, monkeys treated with rotenone selectively accumulated Tf, and there was a tendency for TH immunoreactivity in neurons with heavy Tf accumulation to be reduced. (h) In monkeys, rotenone treatment induced a Tf increase in mitochondria of dopaminergic neurons (panels a and b). Heavy mitochondrial localization of Tf was detectable only in those neurons with high Tf levels (arrow-heads; mitochondrial marker=mitochondrial Heat Shock Protein 60). As noted above, TH levels decreased in Tf-accumulating neurons (panel b).
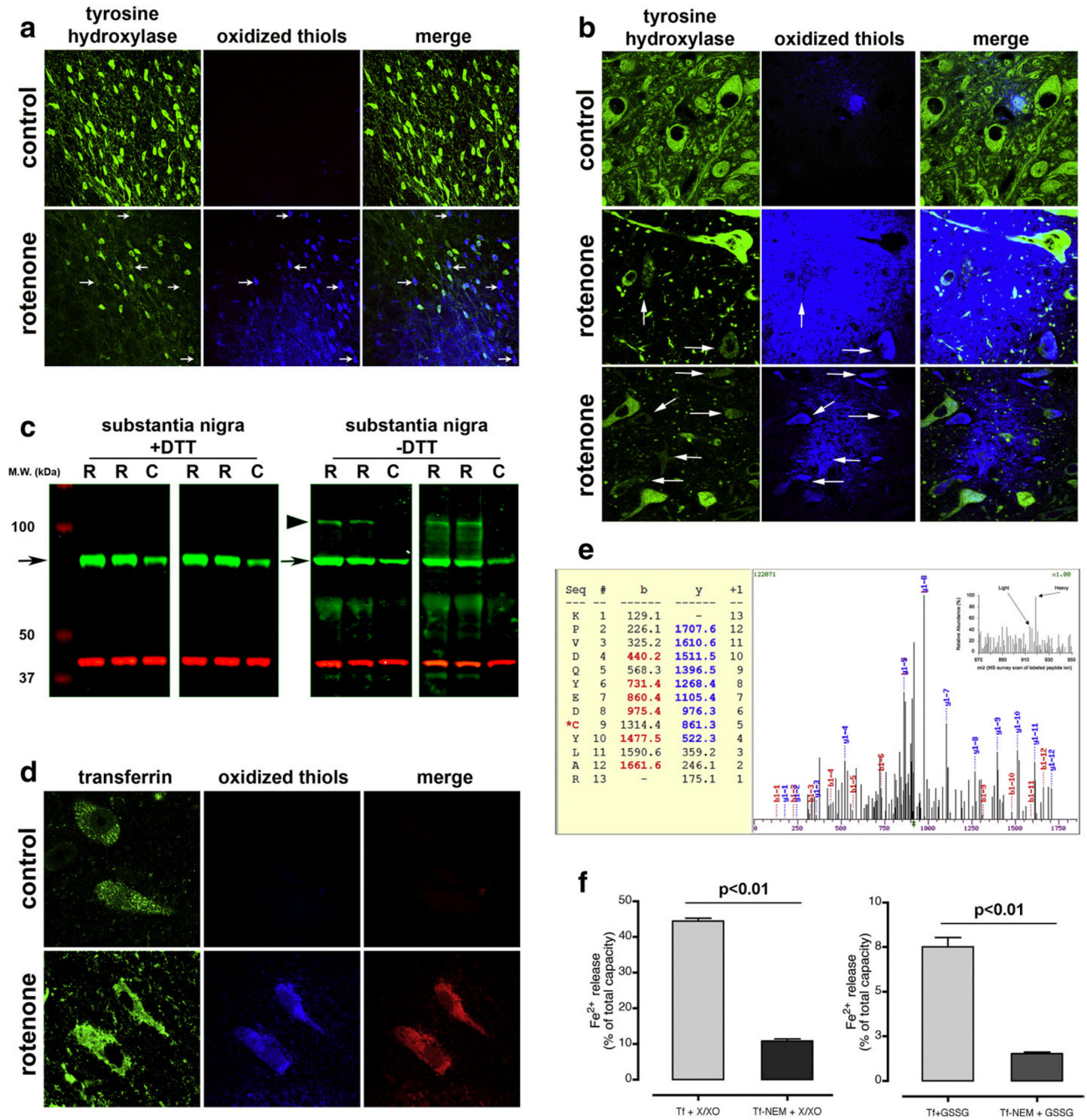
Fig. 3.
Rotenone treatment induces thiol oxidation in substantia nigra dopamine neurons in rats (a) and monkeys (b). As neurons accumulate thiol oxidation, they lose tyrosine hydroxylase immunoreactivity. Neurons with extensive thiol oxidation and reduced tyrosine hydroxylase immunoreactivity are indicated by arrows. (c) Rotenone treatment is associated with the formation of an intermolecular disulfide crosslink between Tf and another protein. Tf from the mitochondrial fraction of substantia nigra was subjected to SDS-PAGE with or without the thiol reducing agent, dithiothreitol (+DTT or −DTT; green band); protein loading was normalized to the 39 kDa subunit of complex I (red band). Under non-reducing conditions (−DTT), specimens from rotenone-treated animals (R) had a highMWband (large arrow-head)

in addition to the normal Tf band (small arrow). The upper band was not seen in control specimens (C) and disappeared under reducing conditions (+DTT). (d) Thiol oxidation of Tf is revealed by FRET. Substantia nigra sections were triple labeled for tyrosine hydroxylase (not shown), Tf and oxidized thiols. In sections from rotenone-treated rats, there was FRET between the fluorescent indicator of oxidized thiols (anilino-naphtalene sulfonate maleimide) and Tf, indicating thiol oxidation of Tf. (e) Identification and quantification of the transferrin peptide KPVDQYEDC*YLAR. The ICAT survey showed that this peptide is increased in the samples from rotenone-treated animals (inset). Because the ICAT reagents label oxidized thiols (heavy ICAT was used for rotenone, light ICAT for control samples), the data indicate higher oxidation of cys260 following rotenone administration. The MS/MS spectrum is a fully tryptic sequence with reasonable matching scores by SEQUEST algorithm (Xcorr=2.3 and ΔCn=0.34). The b and y ions are indicated in the picture. (f) *In vitro* oxidation of Tf through ROS production causes reductive release of ferrous iron (Fe^{2+}) from Tf (left graph). Release of Fe^{2+} from purified $Tf(Fe^{3+})_2$ was assessed by following the absorbance of the Fe^{2+} chelator, bathophenanthroline disulfonate. Under basal conditions, Tf did not release Fe^{2+}. Oxidation of thiols (by formation of a protein-glutathione mixed disulfide; Tf-GSSG) is associated with reduction (Fe^{3+} to Fe^{2+}) and release of iron from Tf (right graph). This reductive release of iron is prevented if thiol groups are alkylated with NEM before incubation with GSSG; alkylation with NEM *per se* did not induce iron release (Supplementary Fig. 5). Values are expressed as percent of total iron capacity; 100% corresponds to the signal detected after – at the end of each experiment – total iron release from Tf was induced through acidification of the solution.
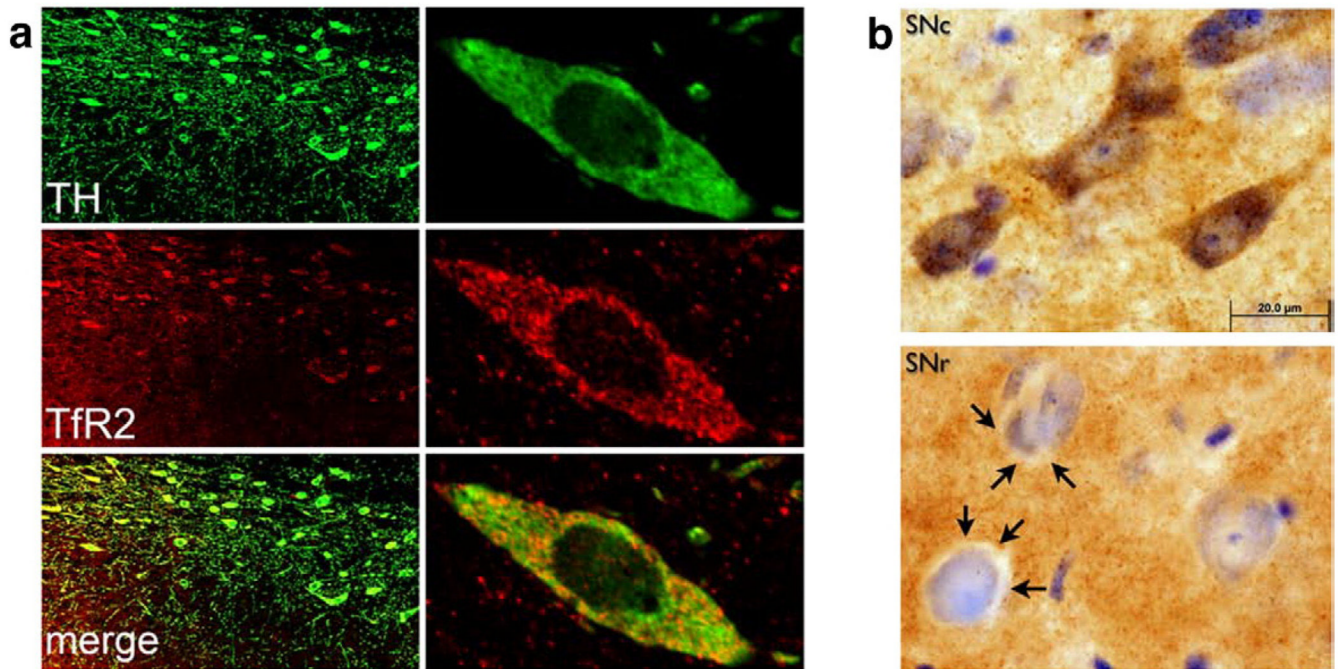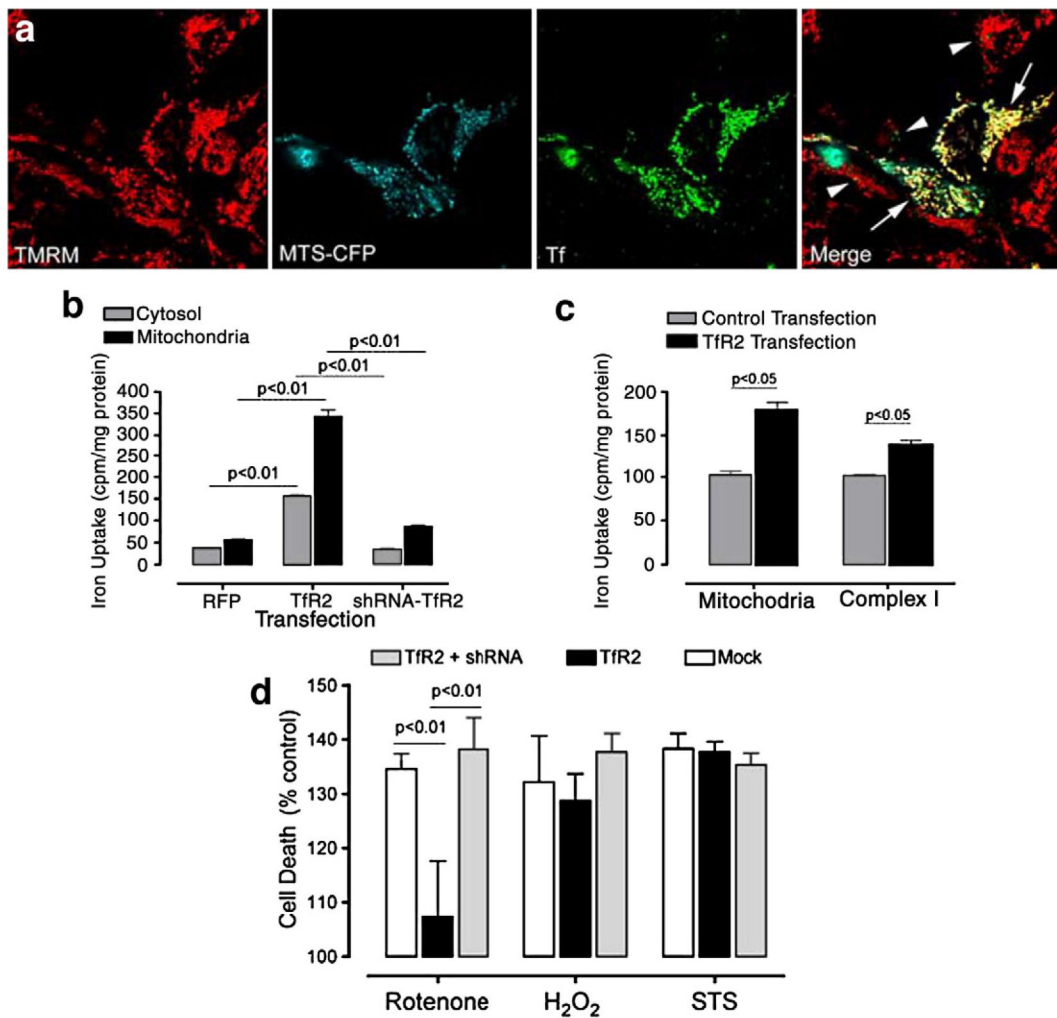
Fig. 4.
(a) TfR2 is colocalized with tyrosine hydroxylase (TH) in dopamine neurons of the substantia nigra, as assessed by laser scanning confocal microscopy. (b) Dopaminergic neurons of the substantia nigra pars compacta (SNc) stain intensely for TfR2, while neurons in the adjacent substantia nigra pars reticulata (SNr) contain little, if any, TfR2. Note the clear cytoplasm (arrows) surrounding neuronal nuclei in SNr, which is in marked contrast to the pattern in SNc. There is also substantial TfR2 immunoreactivity in the neuropil of SNr.
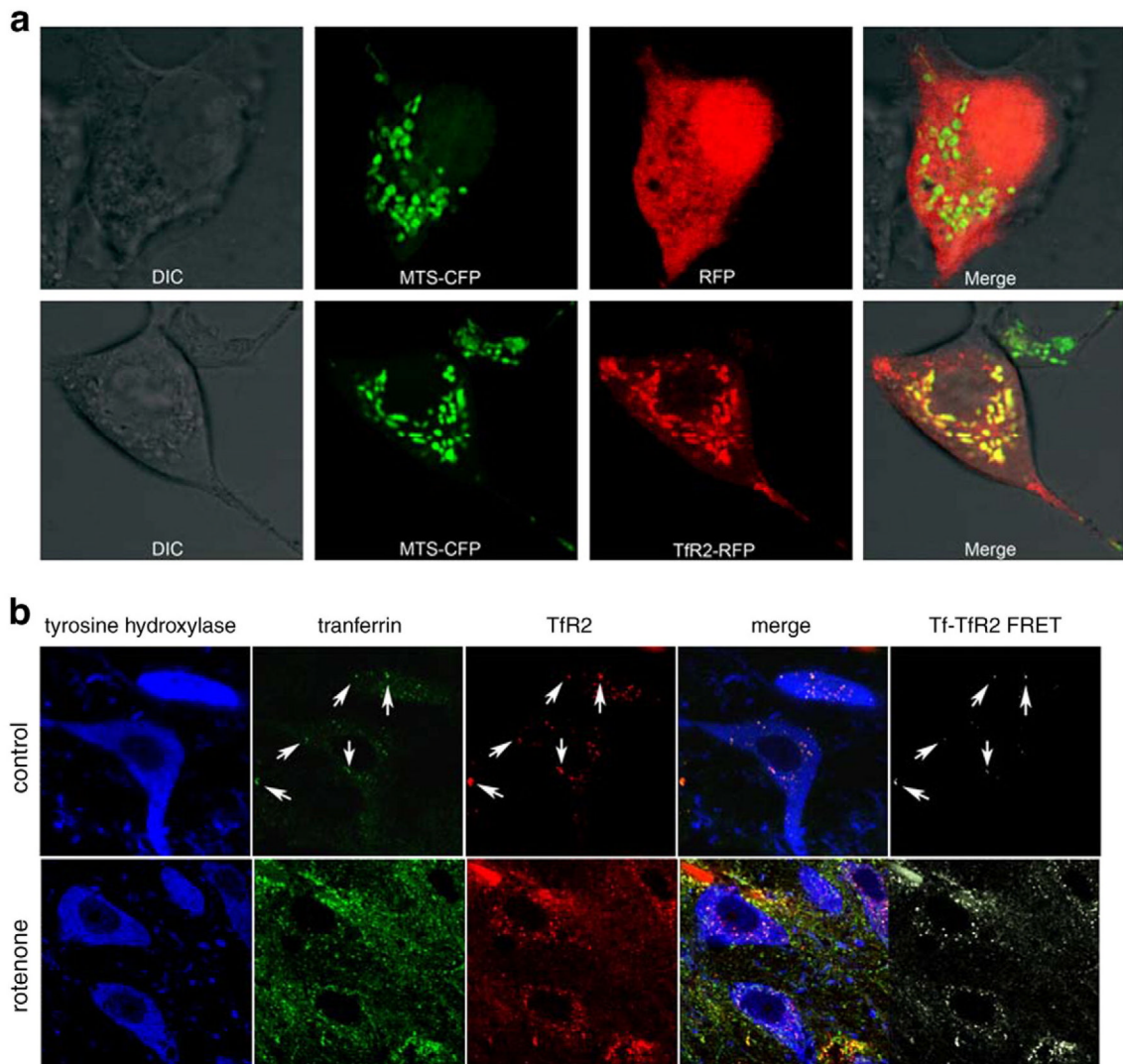
Fig. 5.
(a) The putative mitochondrial targeting sequence (MTS) of TfR2 targets red fluorescent protein (RFP) to mitochondria. Top row, HEK 293 cells were co-transfected with cyan fluorescent protein (CFP) ligated to a known mitochondrial targeting sequence (MTS-CFP) and with RFP. The MTS-CFP protein labeled mitochondria, where as RFP was seen diffusely in the cytosol. A merged image reveals no colocalization of the MTS-CFP and RFP signals. Bottom row, when RFP was ligated to the putative MTS of TfR2 (TfR2-RFP), RFP was directed to mitochondria rather than cytosol, and the merged image showed extensive colocalization with MTS-CFP. The signal of MTS-CFP is represented in the pseudo-color green to better illustrate the yellow-colored overlapping regions in the merge. (b) In dopamine neurons from control animals (top row), there was relatively little expression of Tf and TfR2, but there was substantial colocalization (arrows) – and there was FRET between the two proteins, indicating a physical interaction (molecular proximity) of the proteins. After rotenone treatment (bottom row), there was an increase in the levels of both proteins and the amount of FRET between them also increased. Images from control and rotenone-treated animals were collected using identical parameters. As a result, in the control animals (top row), the Tf and TfR2 signals appear artificially low, so as to avoid saturation of the images from rotenone-treated animals.

Fig. 6.
In cells expressing TfR2, extracellular Tf and iron are taken up and targeted to mitochondria.
(a) HEK 293 cells were co-transfected with TfR2 and MTS-CFP (see Fig. 4)and loaded with
the mitochondrial potentiometric dye, TMRM. All cells were visualized with TMRM, and only
transfected cells were identified by MTS-CFP expression. When fluorescently labeled Tf was
applied extracellularly to the cells, it was rapidly taken up and targeted to mitochondria only
in cells expressing TfR2 (arrows). Only small amount of Tf, which did not colocalize with
mitochondria, were detectable in non transfected cells (arrow-heads). (b) When cells were
transfected with TfR2 (at 50% efficiency), there was a marked, significant increase in
mitochondrial $^{59}[Fe^{3+}]$ uptake, whereas the increase in cytosolic iron was less pronounced. In
this experiment, transfected cells were exposed to $^{59}[Fe^{3+}]_2$-Tf for 1 h, washed, then incubated
for 2 h before fractionation. (c) A portion of the $^{59}[Fe^{3+}]$ that enters mitochondria is
incorporated into complex I, and this is significantly higher inTfR2-transfected cells. In
contrast to the experiment shown in b, these dividing cells were incubated for 16 h prior to
fractionation and immunoprecipitation. (d) Over-expression of TfR2 in SK-N-MC
neuroblastoma cells reduced the toxicity of rotenone, but not H_2O_2 or staurosporine (STS). A
shRNA, which effectively reduces TfR2 protein expression (not shown), blocked this
protective effect. The results represented in the graphs are the average of *n*=3 independent
replicates.
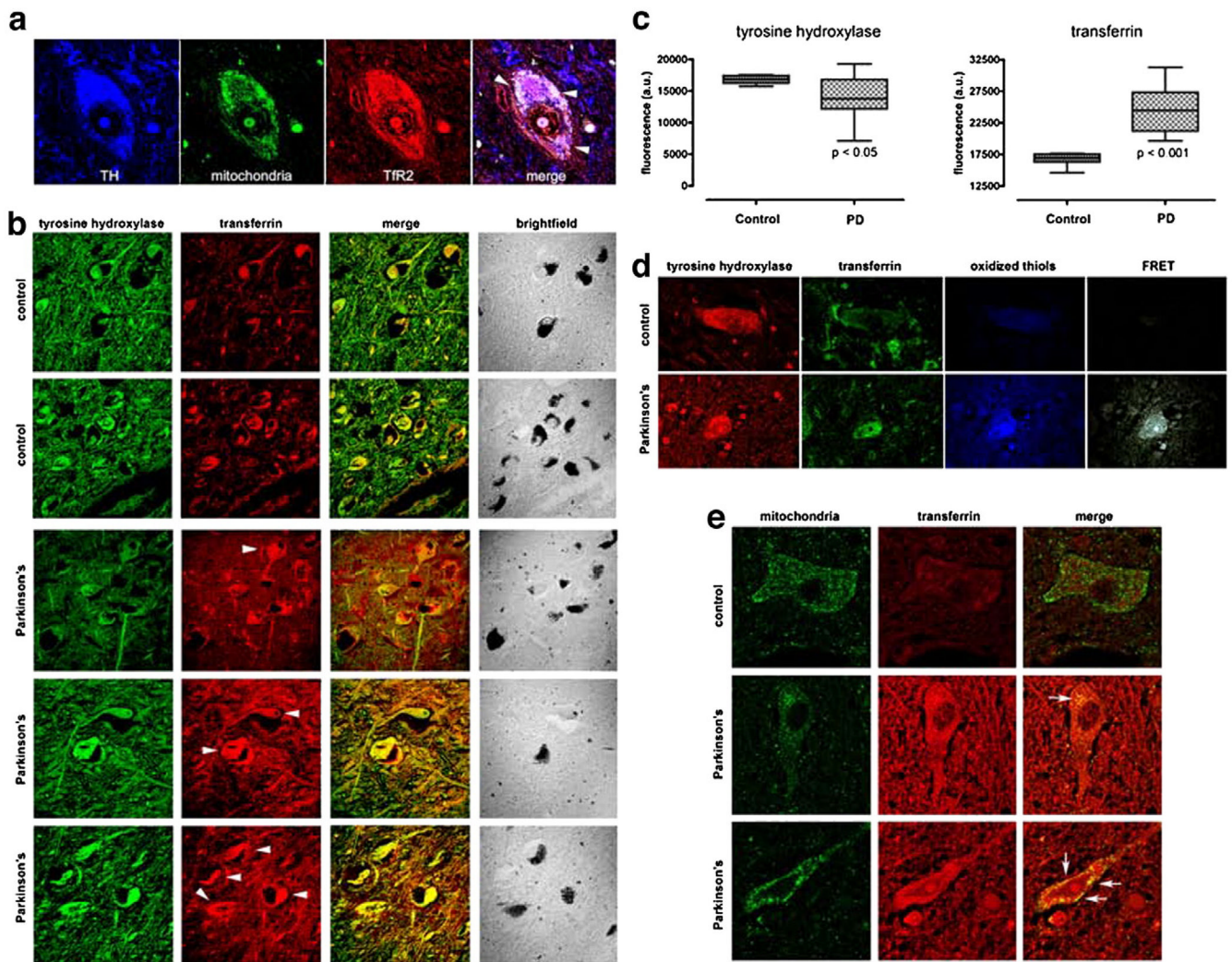
Fig. 7.
(a) As in the rat brain, TfR2 is localized to dopamine neurons in the human brain and it colocalizes, in part, with mitochondria (arrow-heads). (b) There is a marked increase in Tf in substantia nigra dopamine neurons – which contain neuromelanin (brightfield) – and in the surrounding neuropil in Parkinson's disease compared to controls. (c) Quantification of TH and Tf fluorescence intensity in PD cases (n=6) and controls (n=4) reveals that a statistically significant decrease in TH immunoreactivity is paralleled by a significant increase in Tf levels. (d) In Parkinson's disease, there is thiol oxidation of Tf, as indicated by FRET between oxidized thiols (anilino-naphtalene sulfonate maleimide) and Tf (see Fig. 3). (e) In the dopamine neurons, some of the Tf is colocalized with mitochondria. Human substantia nigra sections were triple labeled for tyrosine hydroxylase (not shown), mitochondria and Tf (arrow-heads).